nature cell biology

Flippase-mediated phospholipid asymmetry promotes fast Cdc42 recycling in dynamic maintenance of cell polarity

Arupratan Das[1], Brian D. Slaughter[1], Jay R. Unruh[1], William D. Bradford[1], Richard Alexander[1], Boris Rubinstein[1] and Rong Li[1,2,3]

Lipid asymmetry at the plasma membrane is essential for such processes as cell polarity, cytokinesis and phagocytosis[1–3]. Here we find that a lipid flippase complex, composed of Lem3, Dnf1 or Dnf2 (ref. 4), has a role in the dynamic recycling of the Cdc42 GTPase, a key regulator of cell polarity[5], in yeast. By using quantitative microscopy methods, we show that the flippase complex is required for fast dissociation of Cdc42 from the polar cortex by the guanine nucleotide dissociation inhibitor. A loss of flippase activity, or pharmacological blockage of the inward flipping of phosphatidylethanolamine, a phospholipid with a neutral head group, disrupts Cdc42 polarity maintained by guanine nucleotide dissociation inhibitor-mediated recycling. Phosphatidylethanolamine flipping may reduce the charge interaction between a Cdc42 carboxy-terminal cationic region with the plasma membrane inner leaflet, enriched for the negatively charged lipid phosphatidylserine. Using a reconstituted system with supported lipid bilayers, we show that the relative composition of phosphatidylethanolamine versus phosphatidylserine directly modulates Cdc42 extraction from the membrane by guanine nucleotide dissociation inhibitor.

Establishing stable cell polarity is crucial for cellular morphogenesis and differentiation. The Cdc42 small GTPase localizes to the site of polarized growth in yeast and orchestrates structural and signalling events required for budding and mating[5,6]. Previous work showed that the polarity of Cdc42 distribution is maintained dynamically through two co-localized recycling pathways to counter Cdc42 diffusion[7–9]. Whereas a slow pathway works through actin-based membrane trafficking, a fast pathway is mediated through Rdi1, the yeast guanine nucleotide dissociation inhibitor (GDI) for Rho family GTPases[10]. GDI is known to extract Rho proteins from the membrane by forming a complex involving both protein–protein contacts and binding of GDI to the prenyl lipid anchor at the COOH terminus of these proteins[11,12]. When actin polymerization is inhibited, Rdi1-mediated Cdc42 recycling is required for the polarization of Cdc42 at the presumptive bud site[9].

To gain insights into the molecular mechanisms regulating the location and rate of Rdi1-mediated Cdc42 recycling, we carried out a suppressor screen taking advantage of the fact that overexpression of Rdi1 under the Gal1 promoter represses yeast growth, probably owing to overextraction of Cdc42 and other essential Rho family GTPases from membrane compartments[13] (also see Fig. 1). We reasoned that deletion of a gene encoding a protein that facilitates Cdc42 extraction by Rdi1 might rescue the Gal–Rdi1-induced growth defect. As there are many possible mechanisms for the suppression of the growth defect, the candidates would be further narrowed down to those encoding proteins co-localizing with Cdc42 at the site of polarization. A centromeric plasmid expressing Rdi1 from the Gal1 promoter was transformed into each strain of the yeast haploid non-essential deletion library[14]. Growth of each strain overexpressing Rdi1 was quantified and normalized relative to its growth without Rdi1 overexpression. This screen revealed ~277 initial candidates rescuing the overexpression growth defect, among which 15 encode plasma-membrane-localized proteins (Supplementary Fig. S1b). Among these 15 genes, *LEM3* encodes a protein localized at the site of polarization (Fig. 1a and Supplementary Figs S1a,S2a). Lem3 is a Cdc50 family protein forming a heterodimeric complex with P-type ATPases Dnf1 or Dnf2, which flips aminophospholipid from the outer to inner plasma-membrane leaflet[4,15,16]. Dnf2 was a weak rescuer from the screen (Supplementary Fig. S1a). Both Dnf1 and Dnf2 also localize to the site of polarization, similarly to Lem3 (Supplementary Fig. S2a–c). This observation and their reported involvement in cell polarity[17] led us to carry out an in-depth study on the possible role for aminophospholipid flipping in

[1]Stowers Institute for Medical Research, 1000 East 50th Street, Kansas City, Missouri 64110, USA. [2]Department of Molecular and Integrative Physiology, University of Kansas Medical Center, 3901 Rainbow Boulevard, Kansas City, Kansas 66160, USA.
[3]Correspondence should be addressed to R.L. (e-mail: rli@stowers.org)

Received 7 October 2011; accepted 16 January 2012; published online 19 February 2012; DOI: 10.1038/ncb2444

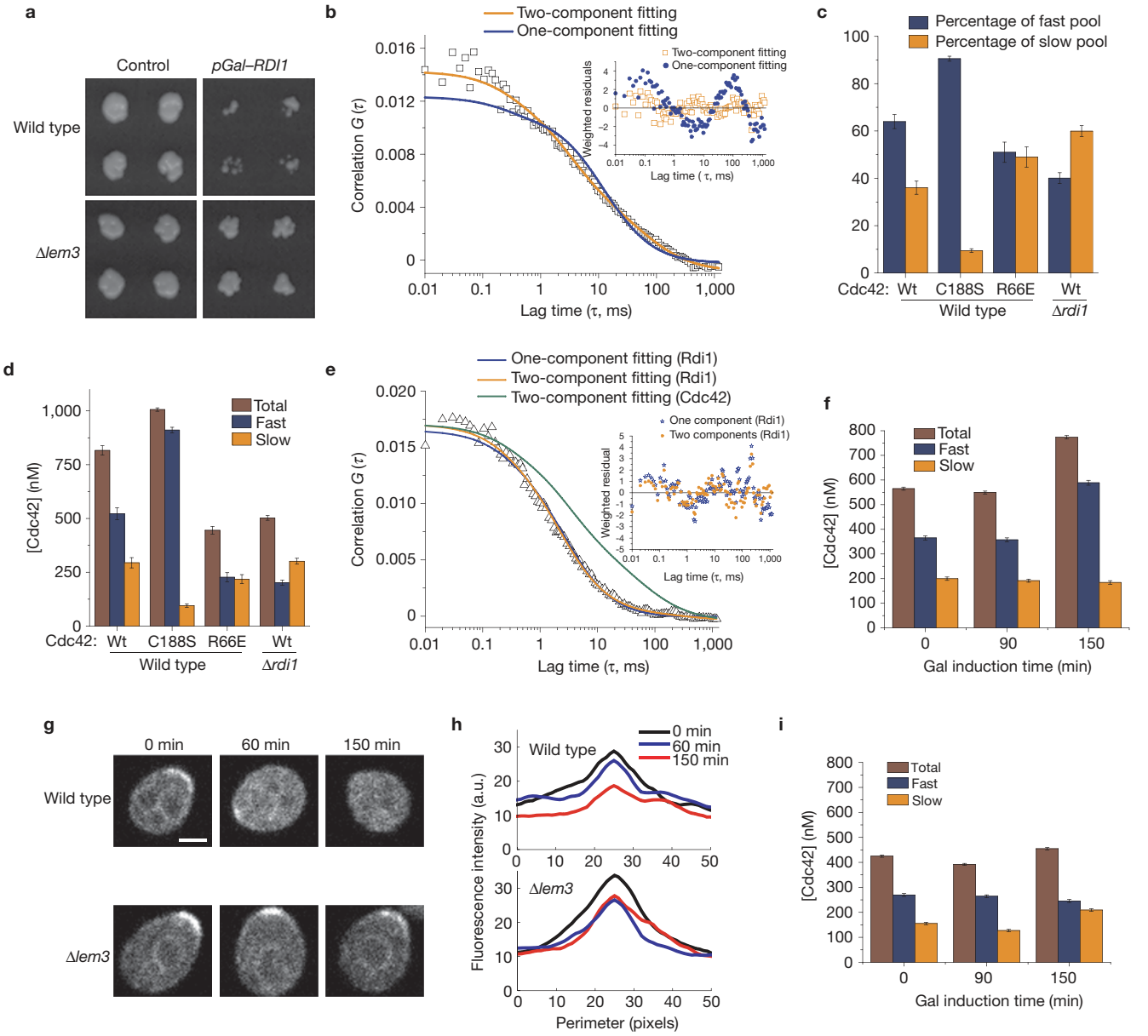

Figure 1 Δ*lem3* suppresses the growth and Cdc42 localization defects due to *RDI1* overexpression. (**a**) Images of wild-type and the Δ*lem3* mutant (four replicate spots) grown on solid media with or without Rdi1 overexpression (*pGal–RDI1*) from the genome-wide screen. (**b**) Example autocorrelation curve of GFP–Cdc42 in wild-type cells under its endogenous promoter. FCS experiments were carried out in live yeast cells (wild type or Δ*rdi1*) expressing GFP-tagged Cdc42, $Cdc42^{R66E}$ or $Cdc42^{C188S}$. FCS data were averaged over 13 cells and fitted with a one-component or two-component diffusion model. Inset: Weighted residuals obtained from each fitting. (**c**) Autocorrelation curves were fitted to a two-component model to extract percentages of slow- and fast-diffusing molecules. Error bars represent the estimated s.e.m. in the parameters determined from fitting average autocorrelation curves obtained from 12, 10, 13 and 22 cells from left to right corresponding to each of the Cdc42 mutants (Methods). Wt, wild type. (**d**) Molar concentration (nM) of soluble Cdc42 calculated from the FCS data as described in **c** (Methods). (**e**) The average autocorrelation curve obtained from FCS experiments in live cells ($n = 12$) expressing Rdi1–mCherry (a red fluorescent protein) was also fitted with one- and two-component models in comparison with the Cdc42 curve. Inset: Distribution of weighted residuals obtained from each fitting. (**f**) Mobile Cdc42 concentrations (nM) of different pools (as indicated) determined at different times of pGal1–Rdi1 induction in wild-type cells. Shown are means and estimated s.e.m. from the analysis of average autocorrelation curves obtained from 21, 26 and 27 cells (from left to right). (**g**) Representative images of GFP–Cdc42 at the polar cap in unbudded wild-type and Δ*lem3* cells at different times of Rdi1 induction (as indicated above each column). Scale bar, 2 μm. (**h**) Fluorescence intensity profiles of GFP–Cdc42 along the perimeter of wild-type or Δ*lem3* cells at different times of *Gal–RDI1* induction. Fluorescence traces from 10–12 cells were first peak-aligned and then averaged to yield each of the profiles shown. (**i**) Same analysis and show as in **f** for Δ*lem3* cells (14, 21 and 23 cells from left to right).

regulating Cdc42 recycling at the polar cortex. To avoid heterogeneity in polarization stages, all the microscopy analyses in this work were carried out with unbudded polarized cells with a Cdc42 polar cap at the incipient bud site.

To test if Δ*lem3* reduces the ability of Rdi1 to extract Cdc42, we first used fluorescence correlation spectroscopy (FCS; ref. 18) to measure the mobile cytosolic concentration of green fluorescent protein (GFP)–Cdc42 expressed under the *CDC42* promoter[7,9] in

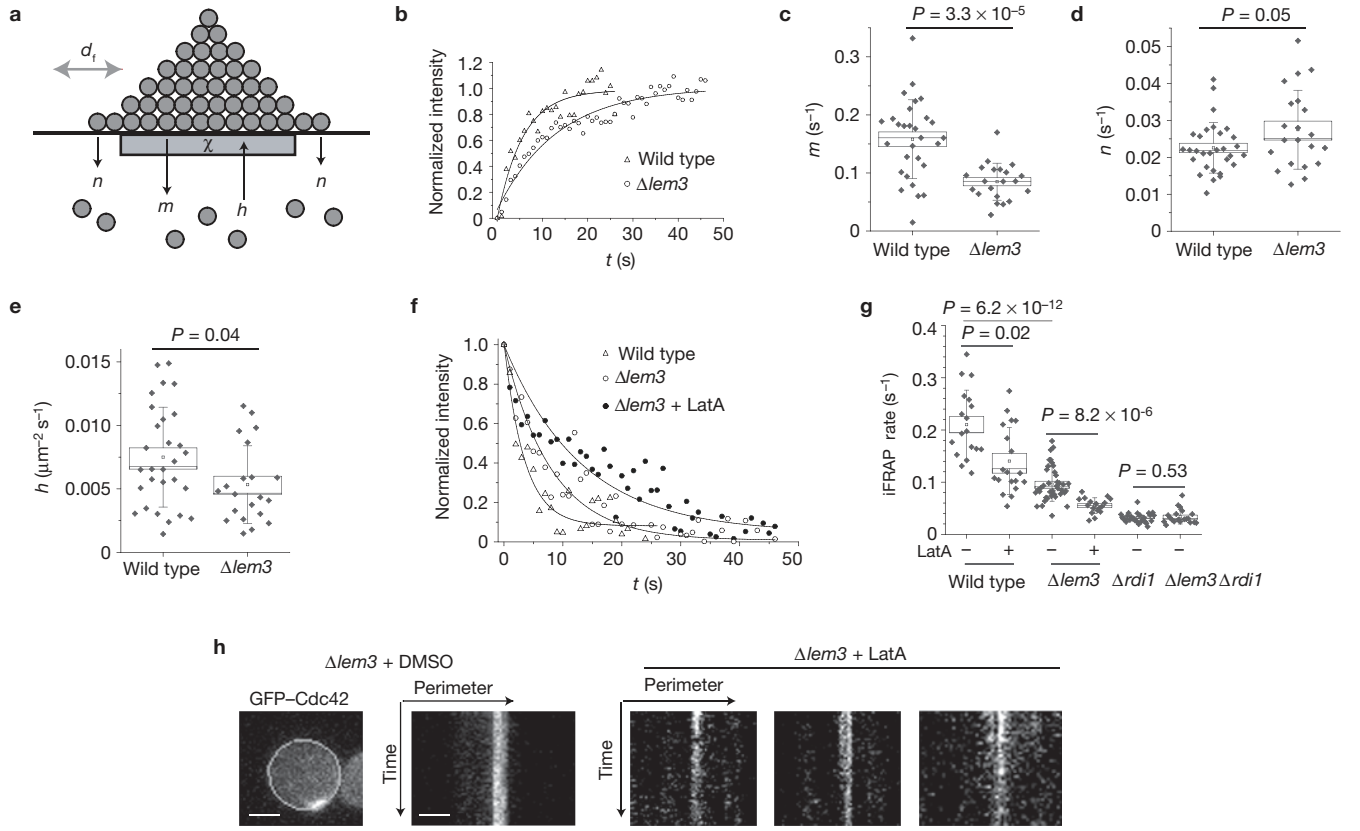

Figure 2 Lem3 regulates Rdi1-mediated Cdc42 internalization and polar-cap morphology. (**a**) Schematic representation of the mathematical model as previously described[9]. The grey horizontal bar represents the overlapping Rdi1 and actin-based delivery window (χ), approximately 25% of the perimeter (Supplementary Fig. S2e–g; ref. 9); d_t, lateral diffusion rate of Cdc42 in the membrane; m and n, internalization rates inside and outside the delivery window, respectively; h, delivery rate inside the window. (**b**) Example normalized FRAP curves of GFP–Cdc42 from wild-type and Δ*lem3* cells. Solid lines represent the exponential fit of the FRAP data. (**c**–**e**) Extracted model parameters from FRAP data. Each point represents a value from a single cell. The small square is the mean; the box range is s.e.m.; whiskers represent s.d.; the line is the median. (**f**) Examples of normalized iFRAP curves from cells expressing GFP–Cdc42. (**g**) iFRAP rates from cells expressing GFP–Cdc42. Box plots are as described in **c**–**e**. (**h**) Example kymographs obtained from bleach-corrected movies (300–385 s long) along the perimeter of Δ*lem3* cells expressing GFP–Cdc42 in the presence of solvent control (dimethylsulphoxide) or 100 μM LatA (three examples shown). Scale bar, 2 μm.

wild-type and Δ*lem3* cells with or without Rdi1 overexpression. FCS records fluorescence intensity fluctuations using a confocal microscope equipped with a photon counter. The autocorrelation curve of these data can be fitted to extract the molar concentration of the diffusing species from the amplitude of the curve (G_0) and the diffusion time (τ_D) from the shape of the curve[18]. Autocorrelation curves of GFP–Cdc42 fitted poorly with a single-component diffusion model but significantly better ($P < 1 \times 10^{-10}$) with a two-component diffusion model (Fig. 1b). This suggests the existence of at least two pools of mobile Cdc42 population, 64% showing fast diffusion ($\tau_D = 2.9 \pm 0.3$ ms) and 36% showing slow diffusion ($\tau_D = 70 \pm 8$ ms; Fig. 1c,d). The fast pool was significantly reduced in the Δ*rdi1* background and for the $Cdc42^{R66E}$ mutant, defective in binding Rdi1 (ref. 19; Fig. 1c,d). The vast majority (>95%) of Rdi1 exists in a fast-diffusing population ($\tau_D = 2.2 \pm 0.1$ ms; Fig. 1e). The slow pool of Cdc42 was diminished by the $cdc42^{C188S}$ mutation (Fig. 1c,d), which prevents prenylation. This analysis, along with the observed *in vivo* cross-correlation of Cdc42 and Rdi1 (ref. 9), suggests that the fast pool of Cdc42 consists largely of the Cdc42–Rdi1 complex, whereas the slow pool is dependent on prenylation and likely to be membrane vesicle associated.

Induction of Rdi1 overexpression resulted in a time-dependent increase in total mobile Cdc42 concentration in the cytosol (Fig. 1f). This increase is accompanied by a similar increase in Cdc42 concentration in the fast but not the slow pool, consistent with extraction of Cdc42 by Rdi1 from the plasma membrane into the soluble pool (Fig. 1f). Consistently, depletion of Cdc42 from the plasma membrane, especially from the polar cortex, can be observed (Fig. 1g,h). In Δ*lem3* cells, the Cdc42 polar cap was more prominent than in wild-type cells before Gal–Rdi1 induction (Fig. 1g,h), accompanied by a smaller mobile Cdc42 pool (Fig. 1i). Whereas Rdi1 overexpression reduced the concentration of Cdc42 in the polar cap of wild-type cells, in Δ*lem3* cells a nearly wild-type pre-extraction level remained (Fig. 1g,h) even after 150 min of Rdi1 induction. The cytosol Cdc42 pool also remained constant (Fig. 1i). As the mean fluorescence intensity of GFP–Cdc42 over the entire cell was slightly reduced in Δ*lem3* when compared with that in wild type (by ~15%, Supplementary Fig. S2d), the reduced Cdc42 soluble pool after 150 min Gal induction in Δ*lem3* (by ~40%, Fig. 1f,i) can be explained as a combined effect of a slightly reduced expression and the reduced extraction from the polar cortex.

We next carried out fluorescence recovery after photobleaching (FRAP) experiments to examine the recycling of GFP–Cdc42 at the

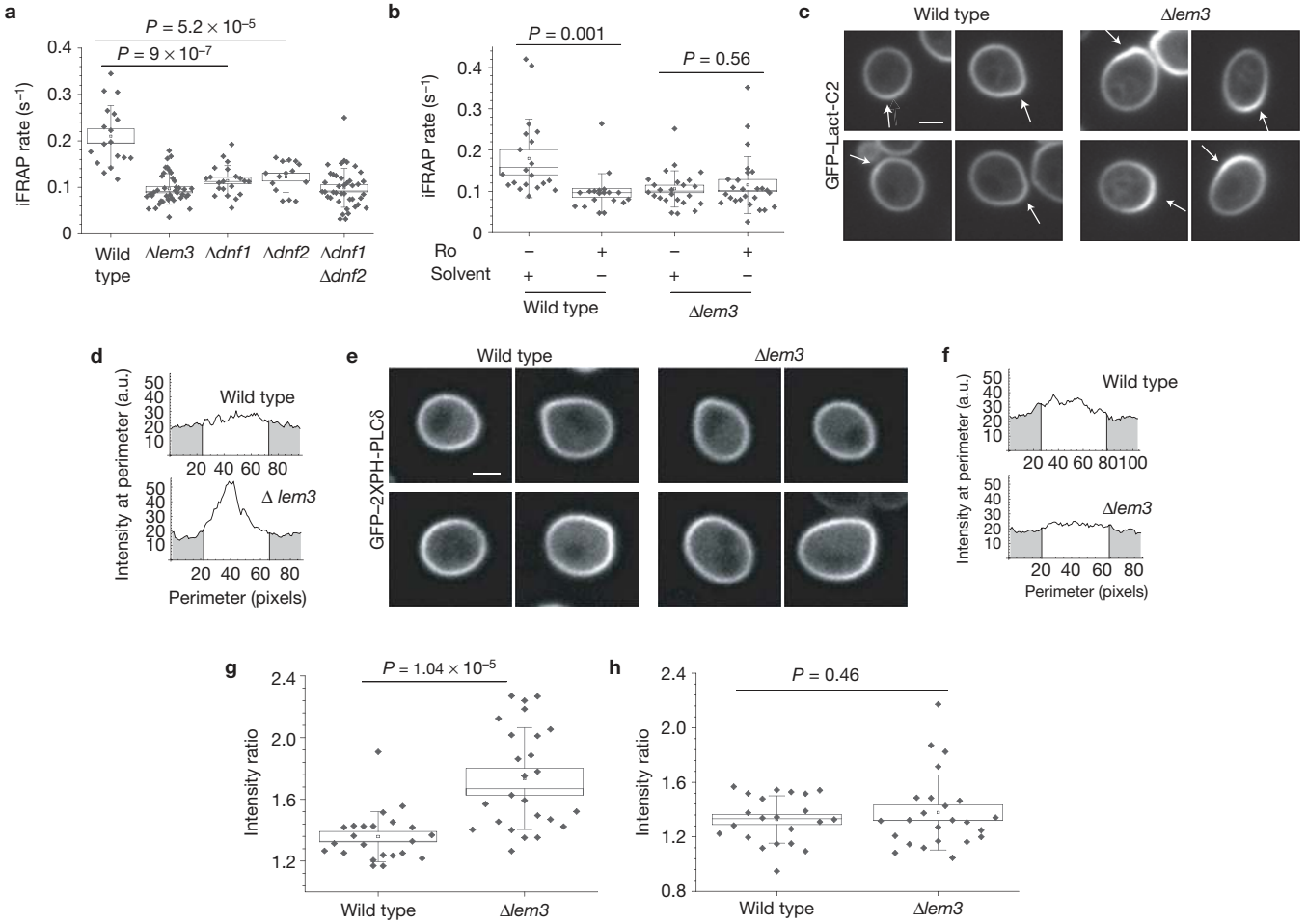

Figure 3 The Lem3–Dnf1/Dnf2 complex regulates the polar Cdc42 dynamics and phosphatidylserine distribution. (**a**) iFRAP rates of GFP–Cdc42 in polarized cells with single or double deletion of *DNF1* and *DNF2* in box plots as described in Fig. 2 caption. (**b**) iFRAP rates shown as in **a** for GFP–Cdc42 in wild-type and Δ*lem3* cells after treatment with 50 μM Ro peptide for 30 min at room temperature. Solvent control was with the same volume of water:acetonitrile (1:1). (**c**) Representative confocal microscopy images of wild-type and Δ*lem3* cells expressing GFP–Lact-C2, a phosphatidylserine biosensor. The white arrows point to the polar caps. Scale bar, 2 μm. (**d**) Representative GFP–Lact-C2 fluorescence intensity traces along the cell perimeter. The white area represents the total fluorescent intensity in the half of the plasma membrane containing the polar cortex; the opposite half is shown in grey. (**e**) Confocal microscopy images of wild-type or Δ*lem3* cells expressing GFP–2xPH-PLCδ (a $PtdIns(4,5)P_2$ biosensor). Scale bar, 2 μm. (**f**) Representative GFP–2xPH-PLCδ fluorescence intensity traces along the cell perimeter as shown in **d**. (**g**) GFP–Lact-C2 fluorescence intensity ratios of the half of the plasma membrane containing the polar cap (white area in **d**) over the rest. The small square is the mean; the box range shows the s.e.m.; the whiskers are the s.d.; the line is the median. (**h**) The GFP-2xPH-PLCδ fluorescence intensity ratio shown as in **g**.

polar cortex[9] and analysed these data using a previously established mathematical model for Cdc42 recycling that enables extrapolation of the rates for Cdc42 dissociation and association from FRAP data[9] (Fig. 2a,b and Supplementary Fig. S2e–g). Model computation found that Δ*lem3* most significantly reduced *m*, the rate of Cdc42 dissociation from the polar-cap region, but only slightly reduced *h*, the rate at which Cdc42 is targeted to the polar cap, whereas *n*, the internalization rate outside the cap, remained similar (Fig. 2c–e). Under such a scenario the model also predicts a slightly more pointed polar cap[9], which could be observed in Δ*lem3* cells (Supplementary Fig. S2h,i). The reduced *m* in Δ*lem3* was confirmed with inverse FRAP (iFRAP), which directly measures the rate of internalization of GFP–Cdc42 at the polar cap[9] (Fig. 2f,g). For comparison, the Cdc42 internalization was not significantly affected by the Δ*pil1* mutation (iFRAP rate of $0.19 \pm 0.028\ s^{-1}$, compared with $0.21 \pm 0.01\ s^{-1}$ in wild type), which disrupts the eisosomes and normal ergosterol distribution in the plasma membrane[20].

To determine whether Δ*lem3* specifically slows down Rdi1-mediated Cdc42 internalization, iFRAP was carried out in the presence of latrunculin-A (LatA), which disrupts endocytosis[21]. LatA further slowed down Cdc42 dissociation in Δ*lem3* to an extent comparable to LatA's effect on wild-type cells (Fig. 2f,g). By contrast, the combined effect of Δ*rdi1* and Δ*lem3* on Cdc42 dissociation rate was non-additive when compared with Δ*rdi1* alone (Fig. 2g). These results suggest that Lem3 selectively promotes Rdi1-mediated Cdc42 dissociation from the polar cortex. LatA treatment also led to marked reduction of polarity in Δ*lem3* cells (Fig. 2h), consistent with a role for Lem3 as an important regulator of Rdi1-mediated Cdc42 recycling in the maintenance of cell polarity.

To test if the flippase complex is involved in fast Cdc42 dissociation from the polar cortex, we carried out iFRAP on Δ*dnf1* and Δ*dnf2* mutant cells. Cdc42 dissociation was significantly slowed in these mutant cells (Fig. 3a). We further tested if acute inhibition of

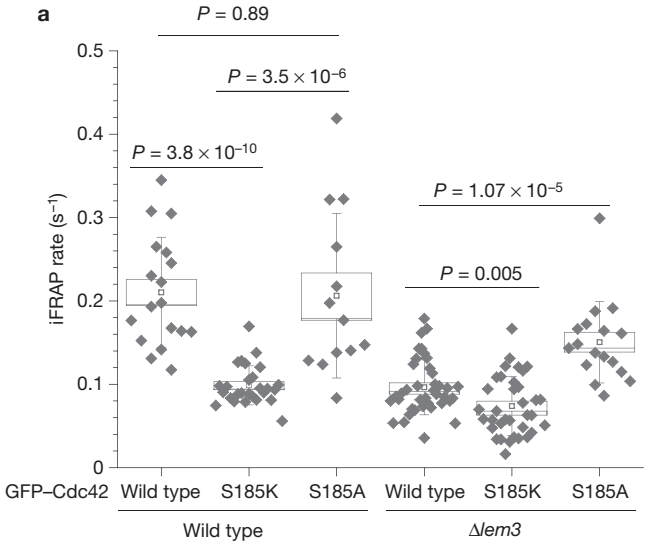

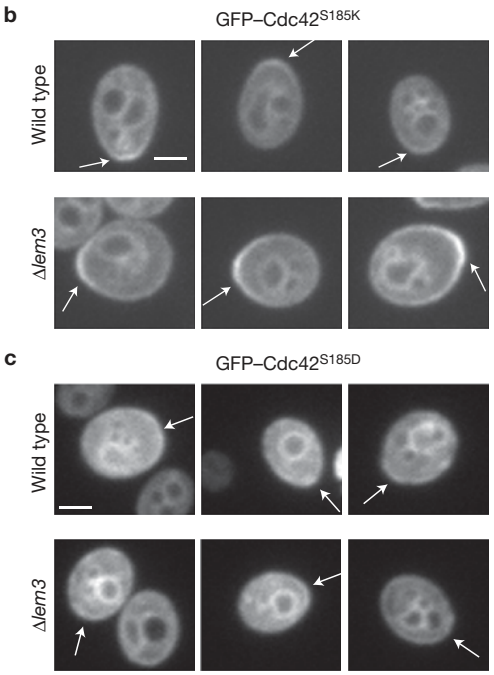

Figure 4 The influence of the charge property of a Cdc42 carboxy-terminal region on Cdc42 dynamics. (**a**) Internalization rates of Cdc42, Cdc42^{S185K} and Cdc42^{S185A} at the polar cortex measured with iFRAP in wild-type and Δ*lem3* cells; box plots as described in Fig. 2 caption. (**b**,**c**) Representative confocal microscopy images of wild-type and Δ*lem3* cells expressing GFP-tagged Cdc42^{S185K} (**b**) or Cdc42^{S185D} (**c**). The white arrows point to the polar caps. Scale bar, 2 μm.

lipid flipping had the same effect by using the tetracyclic peptide Ro09-0198 (Ro, also called cinnamycin), which specifically binds to phosphatidylethanolamine exposed on the outer plasma-membrane leaflet when added to the culture media[1,22]. Ro peptide at 50 μM, which did not cause significant cell death when compared with solvent control (5.6±0.29%, compared with 4.3±0.7%), slowed down Cdc42 dissociation from polar cortex in wild-type cells but not in Δ*lem3* cells (Fig. 3b). These results show that phosphatidylethanolamine flipping is required for fast Cdc42 dissociation from the polar cortex.

Consistent with a previous report[23], a defect in phosphatidylethanolamine flipping in Δ*lem3* correlated with an increase in the negatively charged phospholipid phosphatidylserine at the inner membrane leaflet of the polar cortex, as shown by using the phosphatidylserine biosensor GFP–Lact-C2 (ref. 2; Fig. 3c,d,g and Supplementary Fig. S3a,b). The distribution of phosphatidylinositol 4,5-bisphosphate (PtdIns(4, 5)P_2), monitored with the biosensor GFP-2xPH − PLCδ (PH − PLCδ, pleckstrin homology domain of phospholipase Cδ) (ref. 24), was not significantly different between wild-type and Δ*lem3* cells (Fig. 3e,f,h). As Cdc42 contains a highly conserved cationic tail immediately adjacent to the prenylation site, the slowed Cdc42 dissociation in Δ*lem3* may be due to an enhanced charge interaction between Cdc42 and membrane lipids due to phosphatidylserine enrichment. To test this, we increased the Cdc42 polycationic charge by mutating Ser-185 to lysine (KKS^{185}KK to KKK^{185}KK) and carried out iFRAP on wild-type and Δ*lem3* cells expressing Cdc42^{S185K}. In wild-type cells, the Cdc42^{S185K} dissociation rate from the polar cortex was significantly lower than that of Cdc42, approaching the same slow rate as Cdc42 dissociation in Δ*lem3* (Fig. 4a). In Δ*lem3*, Cdc42^{S185K} also exhibited a moderate but significant decrease in dissociation rate when compared with that of Cdc42 (Fig. 4a). As Ser-185 might possibly act as an electrostatic switch through phosphorylation[25], we also mutated this residue to alanine, but the Cdc42^{S185A} did not exhibit a reduced iFRAP rate when compared with Cdc42 in wild-type cells and even showed a slightly increased iFRAP rate when compared with Cdc42 in Δ*lem3* (Fig. 4a). We also mutated the Ser-185 residue to the negatively charged aspartic acid, and the resulting mutant protein (Cdc42^{S185D}), unlike Cdc42^{S185K}, was poorly localized to the polar cap in both wild-type and Δ*lem3* cells (Fig. 4b,c). These observations support the notion that charge interaction between the Cdc42 polycationic tail and the phospholipids at the polar cortex regulates Cdc42 dissociation from the plasma membrane.

To test if the above regulation is direct, we employed an *in vitro* system involving supported lipid bilayers (SLBs). SLBs were assembled from liposomes with two different lipid compositions, one enriched for phosphatidylserine (referred to as 40% phosphatidylserine, 15% phosphatidylethanolamine, Methods), and the other for phosphatidylethanolamine (referred to as 40% phosphatidylethanolamine, 15% phosphatidylserine). Prenylated Cdc42 with an amino-terminal tetracysteine motif (TC–Cdc42) was purified from a yeast plasma-membrane fraction and labelled with the biarsenical dye FlAsH (ref. 26 and Supplementary Fig. S4). The labelled TC–Cdc42 was added to the SLB and appeared as a fluorescent layer with some bright foci when observed with total internal reflection fluorescence microscopy (TIRF), and its binding to the SLB was dependent on the prenyl group of Cdc42 (Supplementary Fig. S4c–e). In the SLB with 40% phosphatidylserine, 15% phosphatidylethanolamine, the fluorescence intensity of the SLB-bound TC–Cdc42, observed with TIRF, decreased spontaneously and slowly in the presence of the BSA control, and this decay was not enhanced by added purified, bacterially expressed Rdi1 (Fig. 5a,c). In the SLB with 40% phosphatidylethanolamine, 15% phosphatidylserine,

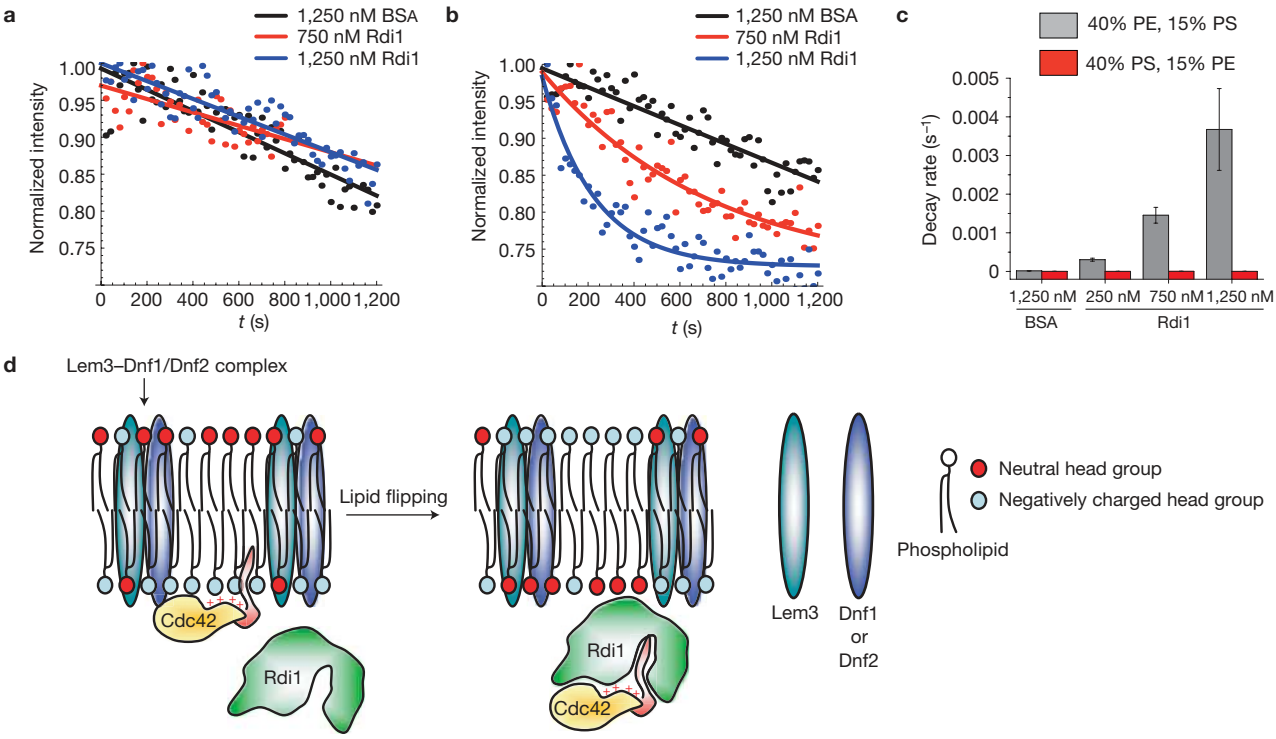

Figure 5 Lipid composition directly regulates Rdi1-mediated Cdc42 extraction. (**a**) Example traces of fluorescence intensity decay due to dissociation of FlAsH-labelled TC–Cdc42 from the SLB containing 40% phosphatidylserine and 15% phosphatidylethanolamine as measured by TIRF microscopy. Fluorescence intensity values (dots) were normalized to the maximum intensity of each trace and fitted to an exponential decay model (lines). (**b**) The same experiment and data presentation as in **a** but from an SLB containing a higher concentration of phosphatidylethanolamine (40%) relative to phosphatidylserine (15%). (**c**) Rates of TC–Cdc42 dissociation from the SLB determined from the TIRF movies, for 40% phosphatidylethanolamine (PE), 15% phosphatidylserine (PS) ($n = 10$, 10, 18 and 18 SLB areas from left to right) and for 40% phosphatidylserine, 15% phosphatidylethanolamine ($n = 10$, 10, 15 and 10 SLB areas from left to right). Bar graphs show mean and s.e.m. (**d**) A schematic model depicting the flippase complex regulating Rdi1-mediated dissociation of Cdc42 from the plasma membrane by changing the charge property of the inner membrane leaflet. On the left, the Cdc42 prenyl group (red) is inserted in the inner leaflet of the plasma membrane at the polar cortex, with electrostatic interaction between the Cdc42 cationic C-terminal region (+) and the negatively charged phospholipid head groups (blue circles) providing stability for this association. The flippase complex mobilizes phospholipids with neutral head groups such as phosphatidylethanolamine from the outer to the inner leaflet, reducing the electrostatic interaction between Cdc42 and the membrane and enhancing the access of Rdi1 to the Cdc42 prenyl group, and thus facilitating the formation of cytosolic Cdc42–Rdi1 complex.

addition of Rdi1 stimulated the dissociation of Cdc42 from the membrane in a dose-dependent manner (Fig. 5b,c), confirming that phosphatidylethanolamine strongly facilitates Rdi1-mediated Cdc42 dissociation from the membrane.

On the basis of the data presented above, we propose a model whereby the Lem3–Dnf1/2 flippase complex acts as an electrostatic switch to promote fast Cdc42 dissociation from the plasma membrane by Rdi1 (Fig. 5d). At the steady state, the polar cortex region is enriched for phosphatidylethanolamine in the outer leaflet and phosphatidylserine in the inner leaflet[2,17]. Such lipid asymmetry facilitates the localization of Cdc42 to the polar cortex[27], possibly by enhancing the charge interaction between the polycationic tail of Cdc42 and the negatively charged membrane surface. A transient increase in neutral lipids such as phosphatidylethanolamine as a result of flippase activity destabilizes the charge interaction of Cdc42 with the inner membrane leaflet, increasing the chance of exposure of the prenyl moiety on Cdc42, thus promoting its capture by the cytosolic Rdi1 protein and fast internalization.

A previous study implicated the Lem3 flippase activity in regulating the activity of the GTPase-activating proteins (GAPs) for Cdc42 and proposed this regulation to be important for the apical to isotropic switch of cell growth at G2/M (ref. 17). Two lines of consideration suggest that the regulation of Cdc42 dynamics observed in our study by the flippase complex is not a result of GAP regulation. First, the conclusion that phosphatidylethanolamine flipping regulates GAP activity in the previous work was based on the *in vitro* demonstration that phosphatidylethanolamine and phosphatidylserine stimulated the GAP activity of Rga1 toward Cdc42, contrasting the inhibitory effect of PtdIns$(4,5)P_2$. However, as shown in this work, the phosphatidylethanolamine-flipping defect in Δ*lem3* is accompanied by an increased enrichment of phosphatidylserine, not PtdIns$(4,5)P_2$, at the inner membrane leaflet of the polar cortex. As phosphatidylserine and phosphatidylethanolamine are equally effective in stimulating Cdc42 GAP *in vitro*[17], the reciprocal enrichment of phosphatidylserine and phosphatidylethanolamine at the inner and outer membrane leaflets in the mutant, respectively, would predict little net effect on the GAP activity. Second, in the previous study the key *in vivo* result supporting the authors' conclusion was that overexpression of the GAP Rga1 rescued the elongated bud morphology in Δ*lem3*, leading to the idea that lipid flipping regulates GAP activity *in vivo*. However, in budded cells beyond the nascent-bud stage, Rga1 is localized at the bud neck[28], whereas Lem3 is found at the bud tip[16]. Thus, it is unlikely that a direct regulation of the GAP by bud-tip-localized

flippase activity underlies the observed genetic interaction. Consistently, Rga1 overexpression does not rescue the defect in Cdc42 dynamics in Δ*lem3* but shows synthetic growth defect with Δ*lem3* (Supplementary Fig. S5a,b). Our model, on the other hand, is based on the change in the charge property of the inner membrane leaflet as a result of phospholipid flipping, and the *in vitro* data support a direct effect of the lipid composition on Cdc42 dissociation by Rdi1. Thus, our study reveals a mechanism by which dynamic lipid asymmetry regulates a highly conserved signalling process during cellular morphogenesis. □

METHODS

Methods and any associated references are available in the online version of the paper at http://www.nature.com/naturecellbiology

Note: Supplementary Information is available on the Nature Cell Biology website

ACKNOWLEDGEMENTS

The authors thank W. Wiegraebe (Stowers Institute for Medical Research) for advice on imaging, K. Lee (Harvard Medical School) for advice on supported lipid bilayer preparation and N. Pavelka for assistance in genome screening data analysis. This study was done to fulfil, in part, requirements for A.D.'s PhD thesis as a student registered with the Open University. This work was supported by NIH grant RO1-GM057063 to R.L.

AUTHOR CONTRIBUTIONS

A.D. and R.L. designed the experiments; A.D. carried out all experiments and prepared the manuscript, with help from B.D.S. and J.R.U.; R.A. and W.D.B. assisted in the whole genome screening; B.R. assisted in data analysis; R.L. conceived and supervised the project and revised the manuscript.

COMPETING FINANCIAL INTERESTS

The authors declare no competing financial interests.

Published online at http://www.nature.com/naturecellbiology
Reprints and permissions information is available online at http://www.nature.com/reprints

1. Iwamoto, K. *et al.* Local exposure of phosphatidylethanolamine on the yeast plasma membrane is implicated in cell polarity. *Genes Cells* **9,** 891–903 (2004).
2. Yeung, T. *et al.* Membrane phosphatidylserine regulates surface charge and protein localization. *Science* **319,** 210–213 (2008).
3. Emoto, K. & Umeda, M. An essential role for a membrane lipid in cytokinesis. Regulation of contractile ring disassembly by redistribution of phosphatidylethanolamine. *J. Cell Biol.* **149,** 1215–1224 (2000).
4. Pomorski, T. & Menon, A. K. Lipid flippases and their biological functions. *Cell Mol. Life Sci.* **63,** 2908–2921 (2006).
5. Etienne-Manneville, S. Cdc42—the centre of polarity. *J. Cell Sci.* **117,** 1291–1300 (2004).
6. Slaughter, B. D., Smith, S. E. & Li, R. Symmetry breaking in the life cycle of the budding yeast. *Cold Spring Harb. Perspect Biol.* **1,** a003384 (2009).
7. Wedlich-Soldner, R., Wai, S. C., Schmidt, T. & Li, R. Robust cell polarity is a dynamic state established by coupling transport and GTPase signaling. *J. Cell Biol.* **166,** 889–900 (2004).
8. Marco, E., Wedlich-Soldner, R., Li, R., Altschuler, S. J. & Wu, L. F. Endocytosis optimizes the dynamic localization of membrane proteins that regulate cortical polarity. *Cell* **129,** 411–422 (2007).
9. Slaughter, B. D., Das, A., Schwartz, J. W., Rubinstein, B. & Li, R. Dual modes of Cdc42 recycling fine-tune polarized morphogenesis. *Dev. Cell* **17,** 823–835 (2009).
10. Masuda, T. *et al.* Molecular cloning and characterization of yeast rho GDP dissociation inhibitor. *J. Biol. Chem.* **269,** 19713–19718 (1994).
11. DerMardirossian, C. & Bokoch, G. M. GDIs: central regulatory molecules in Rho GTPase activation. *Trends Cell Biol.* **15,** 356–363 (2005).
12. Johnson, J. L., Erickson, J. W. & Cerione, R. A. New insights into how the Rho guanine nucleotide dissociation inhibitor regulates the interaction of Cdc42 with membranes. *J. Biol. Chem.* **284,** 23860–23871 (2009).
13. Richman, T. J. *et al.* Analysis of cell-cycle specific localization of the Rdi1p RhoGDI and the structural determinants required for Cdc42p membrane localization and clustering at sites of polarized growth. *Curr. Genet.* **45,** 339–349 (2004).
14. Winzeler, E. A. *et al.* Functional characterization of the *S. cerevisiae* genome by gene deletion and parallel analysis. *Science* **285,** 901–906 (1999).
15. Pomorski, T. *et al.* Drs2p-related P-type ATPases Dnf1p and Dnf2p are required for phospholipid translocation across the yeast plasma membrane and serve a role in endocytosis. *Mol. Biol. Cell.* **14,** 1240–1254 (2003).
16. Kato, U. *et al.* A novel membrane protein, Ros3p, is required for phospholipid translocation across the plasma membrane in *Saccharomyces cerevisiae*. *J. Biol. Chem.* **277,** 37855–37862 (2002).
17. Saito, K. *et al.* Transbilayer phospholipid flipping regulates Cdc42p signaling during polarized cell growth via Rga GTPase-activating proteins. *Dev. Cell* **13,** 743–751 (2007).
18. Slaughter, B. D. & Li, R. Toward quantitative '*in vivo* biochemistry' with fluorescence fluctuation spectroscopy. *Mol. Biol. Cell* **21,** 4306–4311 (2010).
19. Gibson, R. M. & Wilson-Delfosse, A. L. RhoGDI-binding-defective mutant of Cdc42Hs targets to membranes and activates filopodia formation but does not cycle with the cytosol of mammalian cells. *Biochem. J.* **359,** 285–294 (2001).
20. Grossmann, G. *et al.* Plasma membrane microdomains regulate turnover of transport proteins in yeast. *J. Cell Biol.* **183,** 1075–1088 (2008).
21. Ayscough, K. R. *et al.* High rates of actin filament turnover in budding yeast and roles for actin in establishment and maintenance of cell polarity revealed using the actin inhibitor latrunculin-A. *J. Cell Biol.* **137,** 399–416 (1997).
22. Aoki, Y., Uenaka, T., Aoki, J., Umeda, M. & Inoue, K. A novel peptide probe for studying the transbilayer movement of phosphatidylethanolamine. *J. Biochem.* **116,** 291–297 (1994).
23. Stevens, H. C., Malone, L. & Nichols, J. W. The putative aminophospholipid translocases, DNF1 and DNF2, are not required for 7-nitrobenz-2-oxa-1,3-diazol-4-yl-phosphatidylserine flip across the plasma membrane of *Saccharomyces cerevisiae*. *J. Biol. Chem.* **283,** 35060–35069 (2008).
24. Stefan, C. J., Audhya, A. & Emr, S. D. The yeast synaptojanin-like proteins control the cellular distribution of phosphatidylinositol (4,5)-bisphosphate. *Mol. Biol. Cell* **13,** 542–557 (2002).
25. Forget, M. A., Desrosiers, R. R., Gingras, D. & Beliveau, R. Phosphorylation states of Cdc42 and RhoA regulate their interactions with Rho GDP dissociation inhibitor and their extraction from biological membranes. *Biochem. J.* **361,** 243–254 (2002).
26. Griffin, B. A., Adams, S. R. & Tsien, R. Y. Specific covalent labeling of recombinant protein molecules inside live cells. *Science* **281,** 269–272 (1998).
27. Fairn, G. D., Hermansson, M., Somerharju, P. & Grinstein, S. Phosphatidylserine is polarized and required for proper Cdc42 localization and for development of cell polarity. *Nat. Cell Biol.* **13,** 1424–1430 (2011).
28. Caviston, J. P., Longtine, M., Pringle, J. R. & Bi, E. The role of Cdc42p GTPase-activating proteins in assembly of the septin ring in yeast. *Mol. Biol. Cell* **14,** 4051–4066 (2003).

METHODS

Yeast strains and genome-wide screening for suppressors of Gal–Rdi1. A detailed list of yeast strains used in this study is provided in Supplementary Table S1. The yeast haploid non-essential deletion library[14] was transformed with a centromeric plasmid containing Rdi1 under a galactose-inducible promoter (CEN-pGAL-RDI1:His). Cells were grown for 2 days at 30 °C so that all the strains reached maximum growth with approximately the same optical density. At this point, strains were diluted (1:100) and spotted in quadruplicates on Sc + 2% galactose + 2% raffinose (non-transformed control) or Sc − His + 2% galactose + 2% raffinose agar (transformed experimental strains). A His^+ wild-type control strain was included on every plate. A wild-type strain (RLY2530; Wt-control) on non-selective raffinose plates and a wild-type strain with Gal–Rdi1 (RLY3811; Wt-experimental) were included in several plates throughout the library to obtain the wild-type reference value. The plates were incubated at 23 °C for 98 h before saturation. Growth of each spot from the scanned images was quantified as the area and averaged over four spots to obtain growth for each strain. Area values were normalized with respect to the His^+ wild-type control strain on the same plate. A growth ratio for each deletion strain was then obtained by dividing the normalized growth on the experimental plate by that on the control plate. The growth ratio for the wild-type control obtained by averaging from several plates was 0.26. On the basis of the distribution shown in Supplementary Fig. S1a, strains with a growth ratio equal to or above 0.56 were considered as rescuer candidates. On the basis of gene annotation in the *Saccharomyces* Genome Database, genes encoding proteins involved in the galactose-regulated transcription pathway and gene expression were excluded.

Live-cell imaging and data analysis. FRAP and iFRAP experiments and data analysis were carried out as described[9]. High signal-to-noise ratios for the still images were obtained by summing 20 middle confocal slices of a short movie of 20 frames. Image analysis and data extraction were carried out using ImageJ software; statistical analysis and data plotting were carried out using OriginLab Pro software.

Fluorescence correlation spectroscopy. FCS experiments were carried out as described in ref. 29. In brief, live yeast cells were mounted on coverslips and FCS measurements were taken in the cytosol. GFP–Cdc42 was excited with the 488 nm laser line of a Zeiss Confocor 3 through an HFT 488/561 dichroic. HFT 565 was used as an emission dichroic and BP 505–540 as an emission filter to collect fluorescence data. Autocorrelation curves generated from the data were fitted to a two-component diffusion model[30] with a triplet blinking component of 250 µs (ref. 31). Fitting was carried out using weighted nonlinear least squares[32]. The autocorrelation curves from many short (4 s) data acquisitions were averaged for analysis. Curves that demonstrated bleaching or non-diffusive dynamics as judged by visual inspection of the binned trajectories and individual correlation traces were eliminated from the analysis. Weights were estimated from the s.e.m. at each time lag point. Errors in the fitted parameters were estimated by the Monte Carlo method as the s.d. in fits of 500 simulated correlation curves with Gaussian random errors corresponding to the estimated weights and the observed χ^2 parameter[32]. These errors represent the estimated standard error in the fit parameters. An f-test was carried out to compare the one-component and two-component diffusion models[32]. The two-component model represented a strong improvement in the quality of the fit as judged by the f-test ($P < 1 \times 10^{-10}$) and the visual inspection of quality of the fit and residuals (Fig. 1b). The FCS data obtained from Rdi1–mCherry were also fitted with one- and two-component models. In either case, the autocorrelation curve for Rdi1 is dominated by a rapidly diffusing component (more than 95% of population). An f-test between the models preferred the two-component fit with a P-value of less than 1×10^{-10}. However, given the small amplitude of the slow component, we conclude that it represents a relatively insignificant portion of the Rdi1 population.

For measurements of fast- and slow-pool concentrations in the presence of Gal–Rdi1, it is reasonable to assume that fast and slow diffusion times will remain unchanged. Therefore, the diffusion times were fixed to the values obtained for the wild-type strain at zero time for Gal induction. Indeed, the curves were reasonably well fitted by this model in every case. This allows for unbiased estimation of fast- and slow-pool concentrations as a function of Gal induction time.

From the fitting we obtained G_0, the amplitude of the correlation function at zero time lag, and the average diffusion time τ_D required for the molecules to traverse the focal volume. The average number of molecules (N) present in the focal volume was calculated from

$$N = \gamma / G_0 \quad (1)$$

where γ is the shape factor of the focal volume. For one-photon excitation, the γ-factor is 0.36 (ref. 33). The focal volume was calculated using fluorescein in 0.1 M NaOH with the standard method[33–36].

Modelling. For each cell, the mathematical model was applied for the analysis of the FRAP movie. Model parameters and assumptions are as described previously[9]. Considering the overlapping window size between the actin and Rdi1-based recycling mechanisms, we measured the window size from the formin Bni1 distribution in Δ*lem3* cells (Supplementary Fig. S2e–g) and found it similar to the distribution of Bni1 in wild-type cells[9].

Recombinant protein purifications. We constructed a plasmid with a 'pGAL1-GST–HA–TC–Cdc42' sequence (referred to as TC–Cdc42; GST, glutathione *S*-transferase; HA, haemagglutinin). We used a genetically encoded tetracysteine motif (HRWCCPGCCKTF) (TC; ref. 37) that binds efficiently to the biarsenical dye FlAsH[26], and absorbs at 488 nm and emits at 525 nm. The tagged Cdc42 was overexpressed in yeast to maximize the amount of protein at the plasma membrane and purified from a plasma membrane fraction. Cell fractionation to prepare plasma membrane and protein purification was carried out as previously described[12,38] with modifications. After homogenization of spheroplasts, unlysed cells were pelleted at 400*g* for 10 min. The pellet (P1) obtained at this step was rewashed with 5 ml lysis buffer and the supernatants were pooled (S1). The plasma-membrane-containing S1 pool was centrifuged twice at 158,420*g* for 45 min to pellet plasma-membrane fractions (P2). P2 was resuspended in solubilization buffer (50 mM Tris at pH 7.5, 300 mM NaCl, 5 mM $MgCl_2$, 1% Triton X-100 and 0.8 M sorbitol) and briefly homogenized 15 times on ice, and the resultant solution was incubated under shaking for 45 min at 4 °C. The solution was further centrifuged at 9,000*g* for 20 min and the supernatant (S3) was loaded on glutathione–agarose beads (Sigma, G4510) pre-equilibrated with solubilization buffer. The beads were washed with several column volumes of wash buffer (50 mM Tris at pH 7.5, 300 mM Nacl, 5 mM $MgCl_2$ and 0.1% 3-[(3-cholamidopropyl)-dimethylammonio]-1-propanesulphonate (CHAPS)) supplemented with protease inhibitors, phenylmethylsulphonyl fluoride and dithiothreitol, followed by the elution buffer (Tris-HCl at pH 8.0 and 0.1% CHAPS). TC–Cdc42 was eluted with elution buffer containing 10 mM reduced glutathione (Sigma-Aldrich, G4251). Recombinant non-prenylated Cdc42 was purified from bacteria using a GST tag. For Rdi1 purification, yeast Rdi1 was subcloned into the pET-28a vector with a C-terminal hexahistidine tag. Protein purification was done essentially as previously described[12] with minor modifications.

Liposome preparation. To prepare liposomes we purchased chloroform solutions of porcine brain phosphatidylethanolamine (catalogue no 840022C), porcine brain phosphatidylserine (catalogue no 840032C) and porcine brain phosphatidylcholine (catalogue no 840053C) from Avanti Polar Lipids. Cholesterol was purchased from Nu-Chek Prep, and dissolved in chloroform. Lipids were mixed in a clean glass tube, dried under a gentle stream of nitrogen gas and further dried under vacuum for 1 h. The dried lipid mixture was hydrated and resuspended with TBSM buffer (50 mM Tris, 150 mM NaCl, 5 mM $MgCl_2$ at pH 7.5) to a final concentration of 2 mM (ref. 39) and bath sonicateds for 30 min at 45 °C to produce the final liposome solution[40].

Cdc42 extraction assay using TIRF microscopy. Supported lipid bilayers were prepared on no 1.5 glass coverslips. Coverslips were made hydrophilic with a rinse with a concentrated H_2SO_4 and H_2O_2 (3:1) mixture, thoroughly washed with ultrapure water and dried with a stream of nitrogen gas. Liposomes with the composition 40% phosphatidylserine, 15% phosphatidylethanolamine, 5% phosphatidylcholine and 40% cholesterol, or 40% phosphatidylethanolamine, 15% phosphatidylserine, 5% phosphatidylcholine and 40% cholesterol, were added to this coverslip, incubated for 20 min and washed thoroughly with TBSM buffer. (50 mM Tris, 150 mM NaCl, 5 mM $MgCl_2$, pH 7.5) Prenylated Cdc42 with the tetracysteine FlAsH binding motif was labelled with 166.6 µM FlAsH dye (Invitrogen, catalogue no T34561) for 1 h at room temperature and added to the lipid bilayer at 63–126 nM final concentration, followed by 10 min incubation. Unbound and loosely bound protein was thoroughly washed from the lipid bilayer with TBSM buffer. TIRF imaging was carried out using a Carl Zeiss Axiovert 200 M inverted microscope equipped with the Laser TIRF accessory and a Plan-Apochromat ×100, 1.46 NA objective, and a C9100-13 EM-CCD digital camera from Hamamatsu Photonics. To quantify Cdc42 extraction, rectangular areas excluding the bright foci of Cdc42 aggregates were sampled from each experiment. The fluorescence intensity (I) decay for each area was fitted for to an exponential decay model, $I = A_0 + A_1 \exp(-\alpha t)$, where α is the exponential decay rate, using OriginLabPro software.

Statistical analysis. Statistical differences between two sets of data other than FCS data (see above) were analysed with a two-tailed unpaired Student t-test.

DOI: 10.1038/ncb2444

29. Slaughter, B. D., Schwartz, J. W. & Li, R. Mapping dynamic protein interactions in MAP kinase signaling using live-cell fluorescence fluctuation spectroscopy and imaging. *Proc. Natl Acad. Sci. USA* **104,** 20320–20325 (2007).
30. Kim, S. A., Heinze, K. G. & Schwille, P. Fluorescence correlation spectroscopy in living cells. *Nat. Methods* **4,** 963–973 (2007).
31. Haupts, U., Maiti, S., Schwille, P. & Webb, W. W. Dynamics of fluorescence fluctuations in green fluorescent protein observed by fluorescence correlation spectroscopy. *Proc. Natl Acad. Sci. USA* **95,** 13573–13578 (1998).
32. Bevington, P. & Robinson, D. K. *Data Reduction and Error Analysis for the Physical Sciences* 3rd edn 194–218 (McGraw-Hill, 2003).
33. Thompson, N. L. *Fluorescence Correlation Spectroscopy. Topics in Fluorescence Spectroscopy* 337–378 (Plenum Press, 1991).
34. Coles, B. A. & Compton, R. G. Photoelectrochemical ESR. Part I. Experimental. *J. Electroanal. Chem. Interfacial Electrochem.* **144,** 87–98 (1983).
35. Daly, P. J., Page, D. J. & Compton, R. G. Mercury-plated rotating ring-disk electrode. *Anal. Chem.* **55,** 1191–1192 (1983).
36. Hess, S. T. & Webb, W. W. Focal volume optics and experimental artifacts in confocal fluorescence correlation spectroscopy. *Biophys. J.* **83,** 2300–2317 (2002).
37. Martin, B. R., Giepmans, B. N., Adams, S. R. & Tsien, R. Y. Mammalian cell-based optimization of the biarsenical-binding tetracysteine motif for improved fluorescence and affinity. *Nat. Biotechnol.* **23,** 1308–1314 (2005).
38. Goud, B., Salminen, A., Walworth, N. C. & Novick, P. J. A GTP-binding protein required for secretion rapidly associates with secretory vesicles and the plasma membrane in yeast. *Cell* **53,** 753–768 (1988).
39. Lee, K., Gallop, J. L., Rambani, K. & Kirschner, M. W. Self-assembly of filopodia-like structures on supported lipid bilayers. *Science* **329,** 1341–1345 (2010).
40. Poste, G., Papahadjopoulos, D. & Vail, W. J. *In Methods in Cell Biology* 34–72 (Academic Press, 1976).

DOI: 10.1038/ncb2444

nature cell biology

a

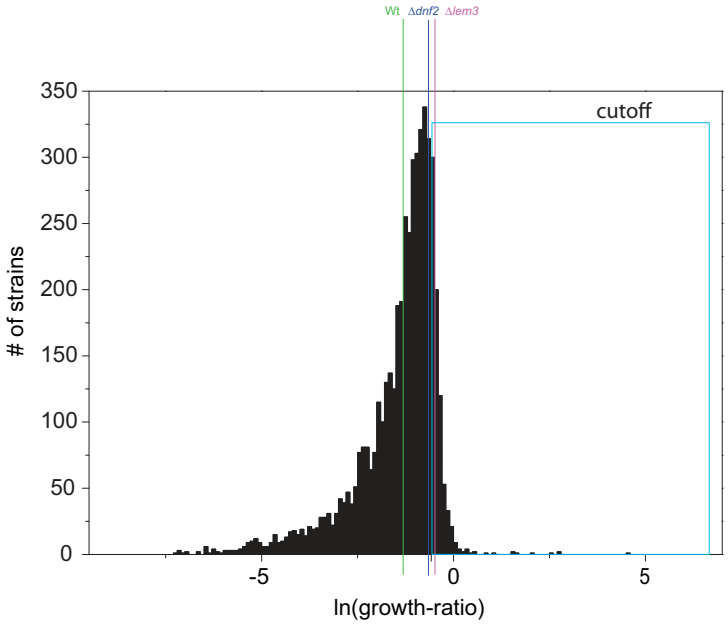

b Rescuer candidates that localize to the plasma membrane.

LEM3	Membrane protein of the plasma membrane and ER, interacts specifically in vivo with the phospholipid translocase (flippase) Dnf1p; involved in translocation of phospholipids and alkylphosphocholine drugs across the plasma membrane.
THI73	Putative plasma membrane permease proposed to be involved in carboxylic acid uptake and repressed by thiamine; substrate of Dbf2p/Mob1p kinase; transcription is altered if mitochondrial dysfunction occurs
PUN1	Plasma membrane protein with a role in cell wall integrity; co-localizes with Sur7p in punctate membrane patches; null mutant displays decreased thermotolerance; transcription induced upon cell wall damage and metal ion stress
FUS1	Membrane protein localized to the shmoo tip, required for cell fusion; expression regulated by mating pheromone; proposed to coordinate signaling, fusion, and polarization events required for fusion; potential Cdc28p substrate
ROD1	Membrane protein that binds the ubiquitin ligase Rsp5p via its 2 PY motifs; overexpression confers resistance to the GST substrate o-dinitrobenzene,zinc, and calcium; proposed to regulate the endocytosis of plasma membrane proteins
SSO1	Plasma membrane t-SNARE involved in fusion of secretory vesicles at the plasma membrane and in vesicle fusion during sporulation; forms a complex with Sec9p that binds v-SNARE Snc2p; syntaxin homolog; functionally redundant with Sso2p
SSO2	Plasma membrane t-SNARE involved in fusion of secretory vesicles at the plasma membrane; syntaxin homolog that is functionally redundant with Sso1p
YPS1	Aspartic protease, member of the yapsin family of proteases involved in cell wall growth and maintenance; attached to the plasma membrane via a glycosylphosphatidylinositol (GPI) anchor
PSR2	Functionally redundant Psr1p homolog, a plasma membrane phosphatase involved in the general stress response; required with Psr1p and Whi2p for full activation of STRE-mediated gene expression, possibly through dephosphorylation of Msn2p
PMP3	Small plasma membrane protein related to a family of plant polypeptides that are overexpressed under high salt concentration or low temperature, not essential for viability, deletion causes hyperpolarization of the plasma membrane potential
YPS3	Aspartic protease, member of the yapsin family of proteases involved in cell wall growth and maintenance; attached to the plasma membrane via a glycosylphosphatidylinositol (GPI) anchor
SNC2	Vesicle membrane receptor protein (v-SNARE) involved in the fusion between Golgi-derived secretory vesicles with the plasma membrane; member of the synaptobrevin/VAMP family of R-type v-SNARE proteins
LDB19	Protein involved in regulating the endocytosis of plasma membrane proteins by recruiting the ubiquitin ligase Rsp5p to its target; localization changes in response to nutrient levels; null mutant has reduced affinity for alcian blue dye
SUR7	Plasma membrane protein that localizes to furrow-like invaginations (MCC patches); component of eisosomes; associated with endocytosis, along with Pil1p and Lsp1p; sporulation and plasma membrane sphingolipid content are altered in mutants
TPN1	Plasma membrane pyridoxine (vitamin B6) transporter; member of the purine-cytosine permease subfamily within the major facilitator superfamily; proton symporter with similarity to Fcy21p, Fcy2p, and Fcy22p

Figure S1 Genome-wide screen for rescuers of Rdi1 over-expression growth defect. (**a**) Distribution of ln(growth-ratio) over the entire yeast haploid non-essential deletion library after 98 hrs of growth at 23C (see Supplementary Methods). Growth ratio is defined as the ratio of growth of a given strain with to without Rdi1 overexpression. Green line represents the Wt value and the cyan box represents the cutoff range of the ln(growth-ratio) for rescuer candidates, including Δlem3 (the pink line). Δdnf2 (blue line) had a slightly lower ln(growth-ratio) than the cutoff and was therefore not in the initial rescuer list. (**b**) A list of the rescuer candidates that localize to the plasma membrane, with SGD description (www.yeastgenome.org).

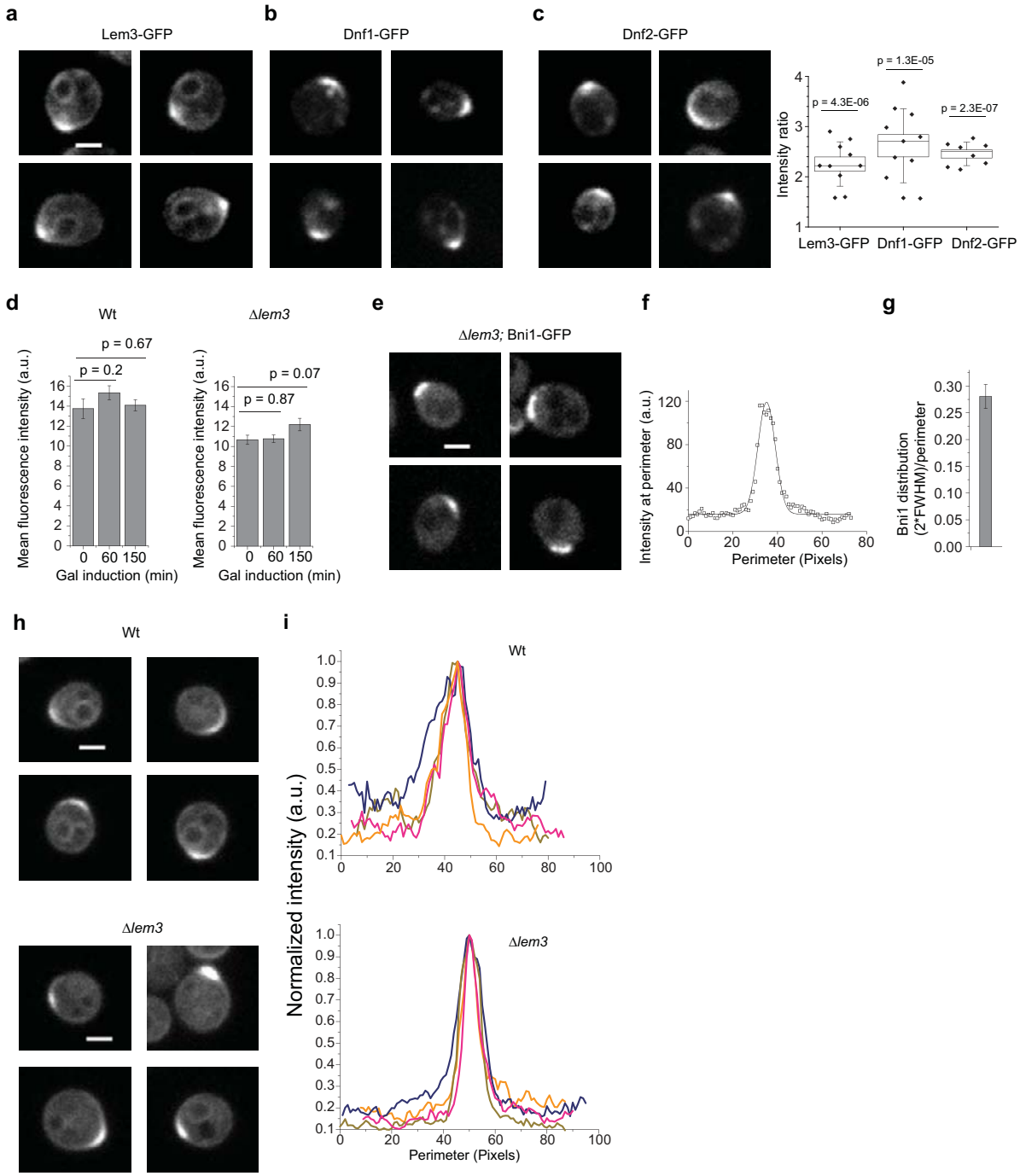

Figure S2 The Lem3 flippase complex is polarized to the polar cortex and the effect of *Δlem3* on the shape of Cdc42 distribution. Shown are confocal images of unbudded polarized cells expressing Lem3-GFP (**a**), Dnf1-GFP (**b**) and Dnf2-GFP (**c**), and box plots for quantification of the fluorescence intensity ratios of the half of the plasma membrane containing the polar cap over the other half as described in Figure 3g legend. P-value is measured using one-tailed one sample t-test to compare whether the intensity ratios are greater than 1.0 which corresponds to uniform distribution. Small Square is the mean; box range shows SEM; whiskers are standard deviation (SD); line is median. (**d**) Quantification of the mean fluorescence intensity over the entire cell for Wt (n = 10, 10, 11, from left to right) and Δlem3 (n = 11, 9, 11, from left to right) cells at different Rdi1 induction time points as indicated. Error bars represent standard error of mean (SEM). (**e**) The delivery window size in Δlem3 was measured by the distribution of GFP tagged formin Bni1 as described previously[1]. Confocal images represent unbudded polarized cells expressing Bni1-GFP. (**f**) The fluorescence distribution along the perimeter was fitted to a Gaussian model. (**g**) The window width is approximated as 2 times the full width half max (FWHM) of the Gaussian distribution. Shown is the mean and SEM (n=16). (**h**) Representative images of GFP-Cdc42 at the polar cap in unbudded Wt and Δlem3 cells. (**i**) Fluorescence intensity traces along the perimeter are normalized and aligned with respect to peak intensity and shown adjacent to each cell type. Scale bar: 2 μm.

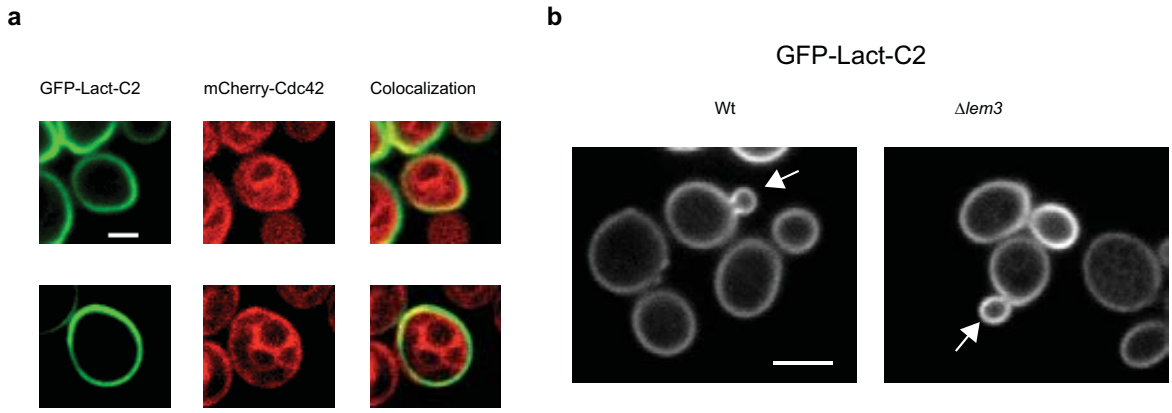

Figure S3 PS polarization overlaps with Cdc42 and PS distribution in budded cells. (**a**) Confocal images of unbudded polarized cells in a cycling population expressing Cdc42 tagged with mCherry at the N-terminus and GFP-Lact-C2. Scale bar: 2 μm. (**b**) Images of budded Wt or Δlem3 cells expressing GFP-Lact-C2. Arrow points to enriched GFP signal in the small buds of Δlem3 cells compared to Wt cells. Scale bar: 4 μm.

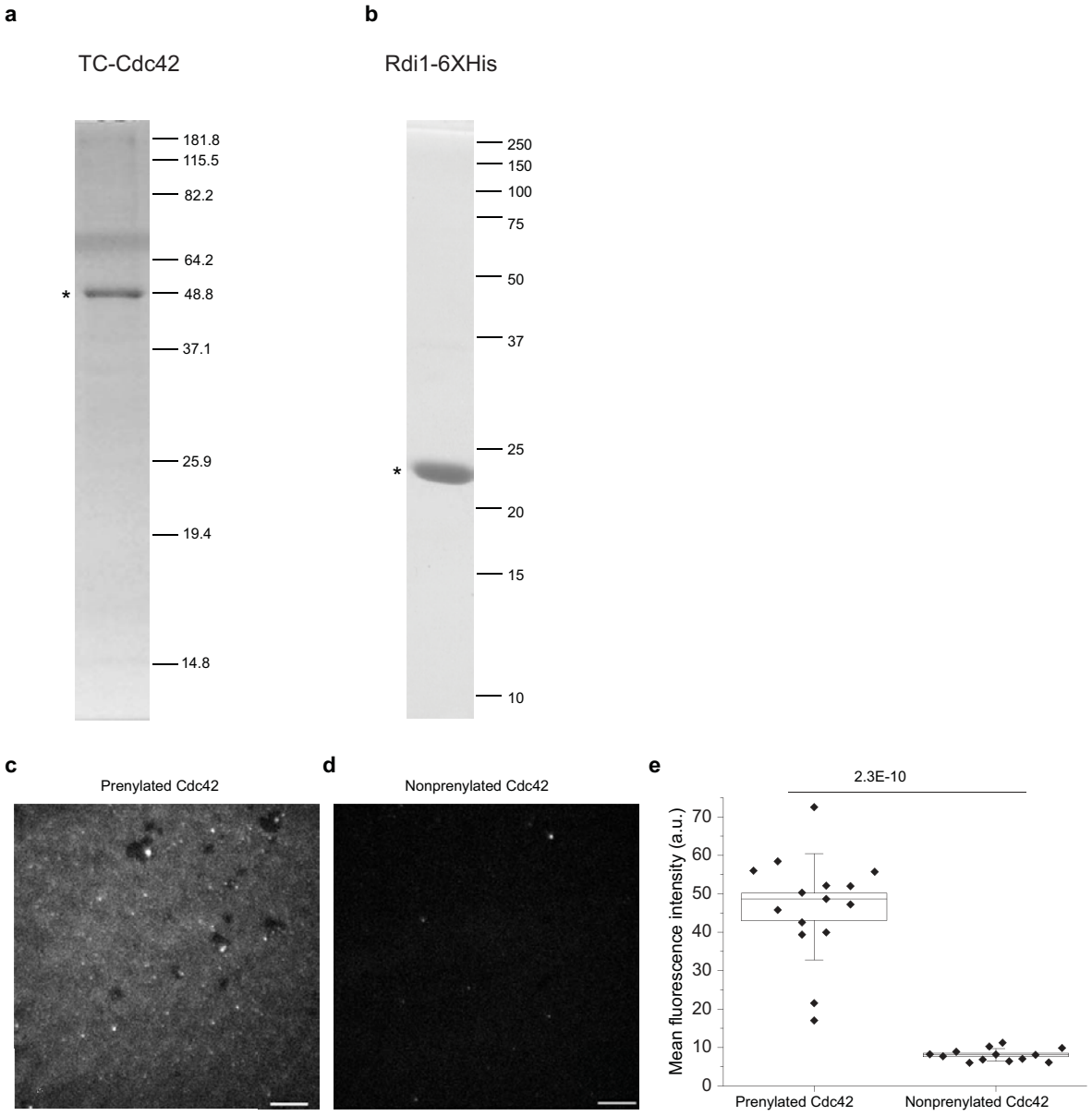

Figure S4 SDS-PAGE followed by Coomassie staining of the purified proteins. Prenyl group is required for TC-Cdc42 association with the SLB. **(a)** Prenylated TC-Cdc42 (GST-HA-TC-Cdc42) protein was expressed and purified from the yeast plasma membrane (See Supplementary method). **(b)** C-terminally hexahistadine-tagged Rdi1 protein was expressed and purified from bacteria cell lysate. Asterisks mark the respective protein band of interest. **(c)** TIRF image of the SLB with 40% PS, 15% PE loaded with 126 nM FlAsH labeled prenylated Cdc42 (purified from yeast plasma membrane). **(d)** SLB with 40% PS, 15% PE similarly labeled as above with 126 nM FlAsSH labeled non-prenylated Cdc42 (purified from bacteria), with the rest of the conditions and image acquisition identical to **c**. Images were presented with identical contrast. Scale bar: 10 μm. **(e)** Mean fluorescence intensity sampled over 13-15 different optical fields on SLBs loaded with FlAsH-labeled prenylated or nonprenylated Cdc42 as explained above. Box plots are shown as described for Figure S2c.

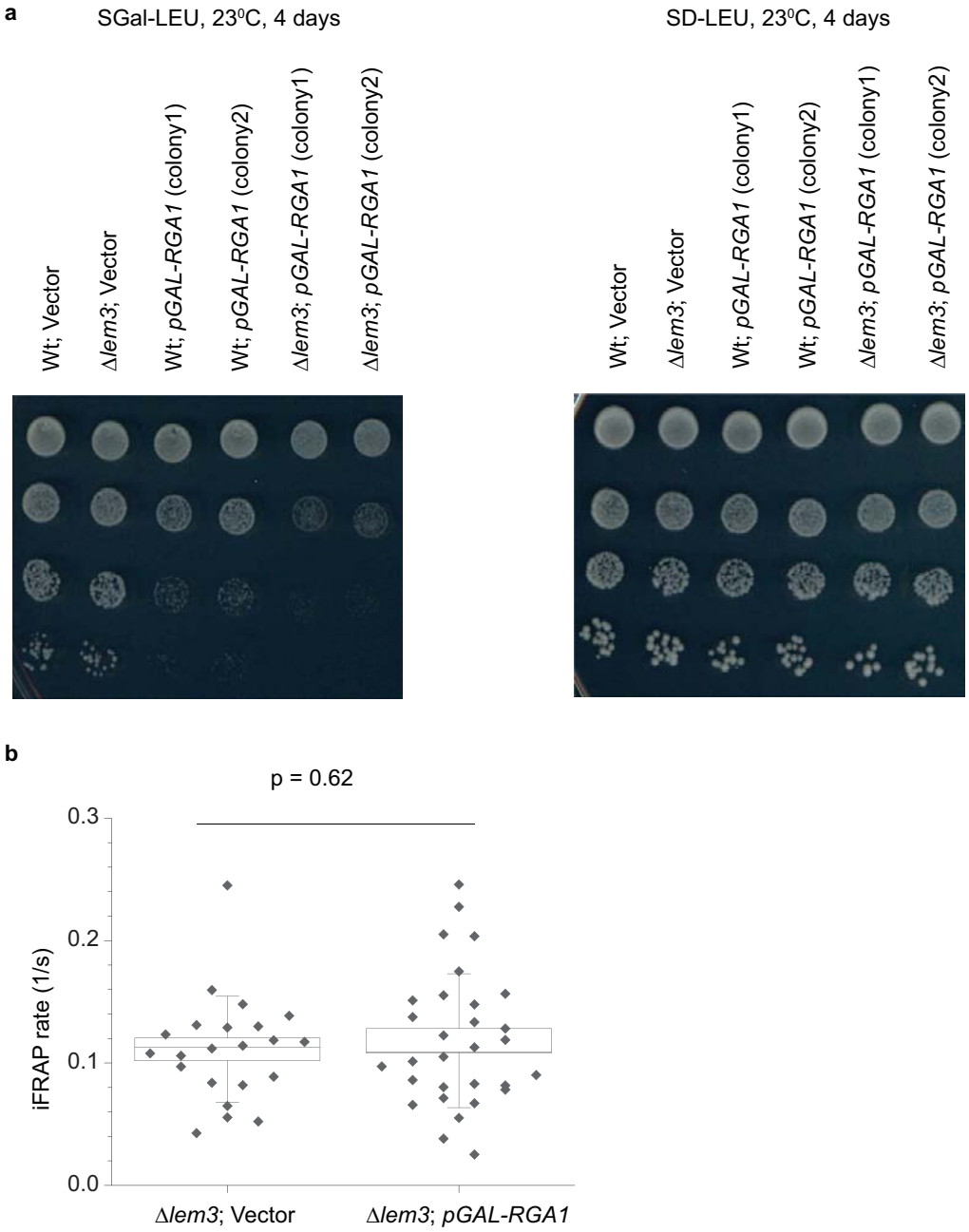

Figure S5 Over-expression of Rga1 (Cdc42 GAP) does not rescue Cdc42 dissociation rate at *Δlem3* polar cortex. **(a)** Serial tenfold dilutions of cultures for the indicated strains were spotted on SGal-Leu and SD-Leu plates. Plates were scanned after 4 days incubation at 23^{0}C. Notice that Rga1 overexpression causes a growth defect, which is exacerbated by Δ*lem3*. (**b**) iFRAP rates (1/s) of GFP-Cdc42 in Δlem3 cells bearing vector control or pGAL1-RGA1. Box plots are shown as described for Figure S2c.

References

1 Slaughter, B. D., Das, A., Schwartz, J. W., Rubinstein, B. & Li, R. Dual modes of Cdc42 recycling fine-tune polarized morphogenesis. Dev. Cell **17**, 823-835 (2009).